Cronfa - Swansea University Open Access Repository

_____

This is an author produced version of a paper published in:
Engineering Computations

_____

Cronfa URL for this paper:
http://cronfa.swan.ac.uk/Record/cronfa45295

_____

_____

High-performance unsymmetric 3-node triangular membrane element with drilling DOFs can correctly undertake in-plane moments

Yan Shang , (State Key Laboratory of Mechanics and Control of Mechanical Structures, College of Aerospace Engineering, Nanjing University of Aeronautics and Astronautics, Nanjing, China)
Song Cen , (Department of Engineering Mechanics, School of Aerospace Engineering, Tsinghua University, Beijing, China, and Key Laboratory of Applied Mechanics, School of Aerospace Engineering, Tsinghua University, Beijing, China)
Zheng-Hua Qian , (State Key Laboratory of Mechanics and Control of Mechanical Structures, College of Aerospace Engineering, Nanjing University of Aeronautics and Astronautics, Nanjing, China)
Chenfeng Li , (College of Engineering, Swansea University, Swansea, UK)

Structured Abstract

Purpose－The paper aims to propose a simple but robust 3-node triangular membrane element with rational drilling DOFs for efficiently analyzing plane problems.

Design/methodology/approach－This new element is developed within the general framework of unsymmetric FEM. The element test functions are determined by using a conforming displacement field which is slightly different with the classical Allman's interpolations, while a self-equilibrated stress field formulated based on the analytical Airy stress solutions is adopted as the trial functions. To ensure the correctness between the drilling DOFs and the true rotations in elasticity, reasonable constraints are introduced through the penalty function method. Moreover, the special quadrature strategy is employed for operating related integrations for future enrichment of element behavior.

Findings－Numerical benchmark tests reveal that this new triangular membrane element has exceptional prediction capabilities. In particular, this element can correctly reproduce a rigid-body rotation motion and correctly undertake the external in-plane twisting moments, thus is a reasonable choice for being used to formulate flat shell elements or to be connected with other kind of elements with physical rotational DOFs.

Originality/value－This work provides a new approach for developing high-performance lower-order elements with simple formulations and good numerical accuracies.

Keywords unsymmetric FEM; membrane element; drilling DOF; physical rotation; in-plane twisting moment

Paper type Research paper

1. Introduction

The finite element method (FEM) is a very powerful numerical tool for engineering and scientific simulations. In many practical applications, lower-order 3-node triangular element and 4-node quadrilateral element are often preferred due to their computation efficiencies. Moreover, triangular elements have more flexibilities than quadrilateral ones in discretization of complex geometries in an automatic manner. However, it is commonly known that lower-order elements are easy to exhibit poor performances because of some inherent deficiencies, such as the sensitivity to mesh distortion and the overestimation of stiffness. Over the past decades, great efforts have been made on overcoming these problems and developing high-performance lower-order elements, namely the element models which have concise formulations and can provide good numerical accuracies with coarse meshes. Nowadays, various new methodologies are still being proposed, such as the hybrid stress-function (HSF) element method (Cen *et al.*, 2011a; Cen *et al.*, 2011b), the smoothed FEM (Liu *et al.*, 2007; Leonetti *et al.*, 2017), the hybrid-EAS method (Vu-Quoc and Tan, 2013), the overlapping element method (Bathe and Zhang, 2017), the elements using the concept of the space fiber rotations (Zouari *et al.*, 2016), the new quasi-conforming elements (Wang *et al.*, 2016; Wang *et al.*, 2017) and so on.

The unsymmetric FEM, which belongs to the Petrov-Galerkin variation method, seems as a promising approach to develop high-performance element models. The first unsymmetric element was an 8-node quadrilateral membrane element named as US-QUAD8 proposed by Rajendran and Liew (2003), which was characterized of employing two different displacement interpolations, i.e., the isoparametric set and metric set, respectively to be the test functions and trial functions. It was reported that this element can maintain good accuracies even in badly distorted mesh, but also found to suffer from some defects, such as the interpolation failure under certain conditions (Prathap *et al.*,

2007). Afterwards, Cen *et al.* (2012) successfully proposed a new methodology by incorporating the novel ideas of the analytical trial function method (Fu *et al.*, 2010) into the original unsymmetric FEM, and subsequently constructed several excellent element models for solving linear and geometric nonlinear problems, including the 8-node and 4-node quadrilateral membrane elements (Cen *et al.*, 2012; Cen *et al.*, 2015; Li *et al.*, 2018) and 8-node hexahedral solid element (Zhou *et al.*, 2017). Their main characteristics were that the elements' trial functions were formulated based on the analytical displacement solutions expressed in Cartesian coordinates or quadrilateral area/hexahedral volume coordinates, which can *a priori* satisfy related governing equations. Recently, Shang and Ouyang (2017) proposed a modified version of Cen's work by directly adopting a stress field, instead of the displacement one, to be the element's trial functions. This stress field was firstly formulated based on the Airy stress solutions and finally determined by using the quasi-conforming theory (Tang *et al.*, 1980). Through this way, they successfully introduced the drilling DOFs into the unsymmetric FEM and developed a 4-node 12-DOF quadrilateral membrane element exhibiting exceptional performance in rigorous tests.

The idea of employing the rotation or drilling DOFs to effectively improve the performances of lower-order membrane elements can be traced back to 1960s. The first remarkable work was devised by Allman (1984), in which the element side displacement was interpolated as a quadratic function by using the vertex rotations. Since then, a great number of papers on this topic have appeared and various elements with Allman-type drilling DOFs were proposed. Some recent attempts include but are not limited to (Bucher, 2018; Leonetti *et al.*, 2017; Boutagouga, 2017; Boutagouga and Djeghaba, 2016; Shin and Lee, 2014; Wisniewski and Turska, 2012). However, it should be noted that, the Allman-type drilling degree is not the Cauchy continuum rotation and has no definite physical interpretations. Therefore, when membrane element with Allman-type drilling DOFs is used to formulate flat shell elements or connected with other kind of elements with physical rotational DOFs, such as beam elements, it may fail in correctly undertaking and carrying over the in-plane twisting moment, leading to unexpected wrong simulation responses. Huang *et al.* (2010) has developed a triangular element model in which special measures are taken to effectively ensure these correctness. However, their element's performance is not very satisfactory.

The purpose of this article is to propose a simple but robust 3-node triangular element with rational drilling DOFs for analysis of plane problems. This new element, denoted as US-T3θ, is

constructed within the modified framework of unsymmetric FEM proposed by Shang and Ouyang (2017). Firstly, an elegant displacement field, which is slightly different with the classical Allman's interpolation, is employed to be the element's test function. Secondly, a self-equilibrated stress field expressed in Cartesian coordinates, which is also well designed based on the Airy stress solutions and the quasi-conforming theory (Tang *et al.*, 1980), is directly adopted to be the trial function. Finally, by the use of the penalty function, reasonable constraints suggested by Huang *et al.* (2010) are introduced for establishing the relationships between the drilling DOFs and the true rotations in elasticity. Besides, for further enrichment of the element behavior, the special quadrature strategy is employed for operating related integrations. Several well-established validation benchmarks are tested and the numerical results verify that this newly formulated element has quite satisfactory prediction capabilities, in many cases, superior to other triangular elements found in the literatures. In particular, it can correctly reproduce a rigid body rotation motion and correctly undertake the external in-plane twisting moments.

2. Finite element formulations

For the new 3-node triangular membrane element, as shown in Figure 1, the element nodal DOF vector is

$$\mathbf{q}^e = \begin{bmatrix} u_1 & v_1 & \theta_1 & u_2 & v_2 & \theta_2 & u_3 & v_3 & \theta_3 \end{bmatrix}^{\mathrm{T}}. \tag{1}$$

2.1 Variation principle and basic element formulations

This new unsymmetric triangular element is developed by following the general procedure proposed by Shang and Ouyang (2017), in which the derivations begin with the principle of virtual work:

$$\iint_\Omega \delta \tilde{\boldsymbol{\varepsilon}}^{\mathrm{T}} \hat{\boldsymbol{\sigma}} t \, \mathrm{d}\Omega - \iint_\Omega \delta \tilde{\mathbf{u}}^{\mathrm{T}} \mathbf{f} t \, \mathrm{d}\Omega - \int_\Gamma \delta \tilde{\mathbf{u}}^{\mathrm{T}} \mathbf{R} t \, \mathrm{d}\Gamma = 0 \,, \tag{2}$$

where Ω is the elastic body with thickness t bounded by Γ; $\tilde{\mathbf{u}}$ is a conforming displacement field, which acts as the test function, and can be interpolated by nodal DOFs:

$$\tilde{\mathbf{u}} = \begin{Bmatrix} \tilde{u} \\ \tilde{v} \end{Bmatrix} = \tilde{\mathbf{N}} \mathbf{q}^e \,; \tag{3}$$

$\tilde{\boldsymbol{\varepsilon}}$ is the strain produced by $\tilde{\mathbf{u}}$:

$$\tilde{\mathbf{\varepsilon}} = \left\{ \begin{array}{c} \tilde{\varepsilon}_x \\ \tilde{\varepsilon}_y \\ \tilde{\gamma}_{xy} \end{array} \right\} = \tilde{\mathbf{B}} \mathbf{q}^e \, ; \tag{4}$$

$\hat{\mathbf{\sigma}}$ is the independently assumed stress trial field and can be written as:

$$\hat{\mathbf{\sigma}} = \hat{\mathbf{S}} \mathbf{q}^e \, ; \tag{5}$$

$\mathbf{R}$ and $\mathbf{f}$ respectively are the prescribed surface traction and body load. Then, substitutions of Equations (3) to (5) into Equation (2) yield the element stiffness matrix

$$\mathbf{K}^e = \iint_{\Omega} \tilde{\mathbf{B}}^{\mathrm{T}} \hat{\mathbf{S}} t \mathrm{d}\Omega , \tag{6}$$

and the equivalent nodal load vector

$$\mathbf{P}^e = \iint_{\Omega} \tilde{\mathbf{N}}^{\mathrm{T}} \mathbf{f} t \mathrm{d}\Omega + \int_{\Gamma} \tilde{\mathbf{N}}^{\mathrm{T}} \mathbf{R} t \mathrm{d}\Gamma \, . \tag{7}$$

2.2 The element's test function

In this work, the displacement $\tilde{\mathbf{u}}$ in Equation (3), which should meet the requirements of inter-element compatibilities, will be determined by using the following shape functions:

$$\tilde{\mathbf{N}} = \begin{bmatrix} \tilde{\mathbf{N}}_1 & \tilde{\mathbf{N}}_2 & \tilde{\mathbf{N}}_3 \end{bmatrix}, \tag{8}$$

with

$$\tilde{\mathbf{N}}_i = \begin{bmatrix} L_i & 0 & -\dfrac{2}{3} L_i (y - y_i) \\ 0 & L_i & \dfrac{2}{3} L_i (x - x_i) \end{bmatrix}, \quad i = 1 \sim 3, \tag{9}$$

in which (x, y) are the Cartesian coordinates of an point and (L_1, L_2, L_3) are the corresponding triangle area coordinates; (x_i, y_i) are the Cartesian coordinates of the node i. Accordingly, the matrix $\tilde{\mathbf{B}}$ in Equation (4) is

$$\tilde{\mathbf{B}} = \begin{bmatrix} \tilde{\mathbf{B}}_1 & \tilde{\mathbf{B}}_2 & \tilde{\mathbf{B}}_3 \end{bmatrix}, \tag{10}$$

with

$$\tilde{\mathbf{B}}_i = \begin{bmatrix} L_{i,x} & 0 & -\dfrac{2}{3} L_{i,x} (y - y_i) \\ 0 & L_{i,y} & \dfrac{2}{3} L_{i,y} (x - x_i) \\ L_{i,y} & L_{i,x} & \dfrac{2}{3} L_{i,x} (x - x_i) - \dfrac{2}{3} L_{i,y} (y - y_i) \end{bmatrix}, \quad i = 1 \sim 3 . \tag{11}$$

It should be pointed out that, if the coefficient 2/3 in Equation (9) is replaced by 1/2, this displacement will coincide with the classical Allman's interpolation along the element boundary. Here, the usage of 2/3 instead of 1/2, as suggested by Huang *et al.* (2010), is to make it possible for the element's drilling DOFs to correctly present the true rotations in elasticity.

2.3 The element's trial function

As discussed above, in the approach proposed by Shang and Ouyang (2017), the element's trial functions are formulated based on the analytical Airy stress solutions. In this work, the stress trial field of this new nsymmetric triangular element will be obtained in the same manner.

Firstly, the stress field $\hat{\boldsymbol{\sigma}}$ in Equation (5) is assumed as

$$\hat{\boldsymbol{\sigma}} = \mathbf{H}\boldsymbol{\alpha},\tag{12}$$

with

$$\mathbf{H} = \begin{bmatrix} 0 & 0 & 2 & 0 & 0 & 2x & 6y \\ 2 & 0 & 0 & 6x & 2y & 0 & 0 \\ 0 & -1 & 0 & 0 & -2x & -2y & 0 \end{bmatrix},\tag{13}$$

$$\boldsymbol{\alpha} = \begin{bmatrix} \alpha_1 & \alpha_2 & \cdots & \alpha_7 \end{bmatrix}^{\mathrm{T}}.\tag{14}$$

Note that each column of above matrix $\mathbf{H}$ is one set of analytical stress solutions of the plane problem which are derived by using the concept of Airy stress function. Therefore, the stress field in Equation (12) can *a prior* satisfy related governing equations.

Next, to get the relationship between the unknown coefficients $\boldsymbol{\alpha}$ and the element nodal DOFs $\mathbf{q}^e$, the quasi-conforming technique will be applied to this stress field $\hat{\boldsymbol{\sigma}}$ and the strain $\tilde{\boldsymbol{\varepsilon}}$ obtained in Section 2.2:

$$\iint_{\Omega} \mathbf{H}^{\mathrm{T}} \left(\tilde{\boldsymbol{\varepsilon}} - \mathbf{D}^{-1}\hat{\boldsymbol{\sigma}} \right) t \mathrm{d}\Omega = \mathbf{0},\tag{15}$$

with

$$\mathbf{D} = \frac{E'}{1-\mu'^2} \begin{bmatrix} 1 & \mu' & 0 \\ \mu' & 1 & 0 \\ 0 & 0 & (1-\mu')/2 \end{bmatrix},\tag{16}$$

where $E' = E, \mu' = \mu$ for the plane stress problem and $E' = E/(1-\mu^2), \mu' = \mu/(1-\mu)$ for the plane strain problem, in which E and μ respectively are Young's modulus and Poisson's ratio. Then,

by substituting Equation (4) and Equation (12) into Equation (15), we obtain

$$\boldsymbol{\alpha} = \mathbf{M}^{-1}\mathbf{V}\mathbf{q}^e, \tag{17}$$

in which

$$\mathbf{M} = \iint_{\Omega} \mathbf{H}^{\mathrm{T}}\mathbf{D}^{-1}\mathbf{H}t\mathrm{d}\Omega, \tag{18}$$

$$\mathbf{V} = \iint_{\Omega} \mathbf{H}^{\mathrm{T}}\tilde{\mathbf{B}}t\mathrm{d}\Omega. \tag{19}$$

Finally, the matrix $\hat{\mathbf{S}}$ in Equation (5) can be derived by substituting Equation (17) back into Equation (12):

$$\hat{\mathbf{S}} = \mathbf{H}\mathbf{M}^{-1}\mathbf{V}. \tag{20}$$

2.4 One-point quadrature for stiffness matrix

Since the element's test function and trial function have already been determined in previous sections, the element stiffness matrix and the equivalent nodal load vector can be easily calculated by substituting related equations into Equation (6) and Equation (7). Note that, in order to further improve element's behavior, the one-point quadrature strategy is employed for calculating Equation (6), while other integrations are still operated by using the full quadrature scheme.

2.5 The constraints between drilling DOFs and true rotations

As discussed in Section 2.2, to make the new triangular element able to reproduce a rigid rotation motion and correctly undertake the external in-plane twisting moments, the coefficient 2/3 has been used instead of 1/2 in Equation (9). In addition, as suggested by Huang *et al.* (2010), the following constraints should also be applied to the element:

$$\frac{1}{3}\left(\theta_1 + \theta_2 + \theta_3\right) - \frac{1}{2}\left(\frac{\partial v_0}{\partial x} - \frac{\partial u_0}{\partial y}\right) = \mathbf{A}\mathbf{q}^e = 0, \tag{21}$$

with

$$u_0 = L_1 u_1 + L_2 u_2 + L_3 u_3, \quad v_0 = L_1 v_1 + L_2 v_2 + L_3 v_3. \tag{22}$$

From above two equations, the detailed expression of the matrix $\mathbf{A}$ can be obtained:

$$\mathbf{A} = \left[\frac{c_1}{4\Delta} \quad \frac{-b_1}{4\Delta} \quad \frac{1}{3} \quad \frac{c_2}{4\Delta} \quad \frac{-b_2}{4\Delta} \quad \frac{1}{3} \quad \frac{c_3}{4\Delta} \quad \frac{-b_3}{4\Delta} \quad \frac{1}{3}\right]. \tag{23}$$

in which Δ is the area of the triangular element, and

$$b_1 = y_2 - y_3, \quad b_2 = y_3 - y_1, \quad b_3 = y_1 - y_2, \tag{24}$$

$$c_1 = x_3 - x_2, \quad c_2 = x_1 - x_3, \quad c_3 = x_2 - x_1. \tag{25}$$

In this work, the influences of constraints in Equation (21) are considered by using the penalty function method. As a consequence, a penalty stiffness matrix $\mathbf{K}_{\mathrm{C}}^e$ is deduced, which will be added to the stiffness matrix $\mathbf{K}^e$ obtained by Equation (6) to get the final element stiffness matrix $\mathbf{K}_{\mathrm{final}}^e$:

$$\mathbf{K}_{\mathrm{final}}^e = \mathbf{K}^e + \mathbf{K}_{\mathrm{C}}^e, \tag{26}$$

with

$$\mathbf{K}_{\mathrm{C}}^e = \iint_{\Omega} G\mathbf{A}^{\mathrm{T}}\mathbf{A}t\mathrm{d}\Omega, \tag{27}$$

G is the shear elastic modulus.

3. Numerical validations

Six benchmark examples have been carefully chosen to assess this new unsymmetric triangular element's performance. The obtained responses will be compared <mark>with several well-known 3-node 9-DOF elements and 6-node 12-DOF element listed in Table 1.</mark>

3.1 The patch test

As shown in Figure 2, the small patch is modeled by four elements. The displacements at the boundary nodes 1~4, which are calculated by using the following equations, are imposed to this patch as the boundary conditions:

$$u = 10^{-3}(x + y/2), \quad v = 10^{-3}(y + x/2). \tag{28}$$

Correspondingly, the constant stress states are

$$\sigma_x = \sigma_y = 1333.3333, \quad \tau_{xy} = 400.0. \tag{29}$$

<mark>In Table 2, the numerical results obtained by using the mesh shown in Figure 2 are listed. Moreover, some meshes which contain severely distorted elements are also tested and the contour plots of displacement u are presented in Figure 3. It is obvious that this new element can always exactly pass this constant stress patch test.</mark> Thus the computation convergence can be guaranteed.

3.2 The rigid body rotation test

This test was proposed by Huang *et al.* (2010) to verify whether a membrane element with drilling DOFs can correctly reproduce a rigid rotation motion and present the true rotations in elasticity. As shown in Figure 4, a square plate is divided into four elements. Two cases with different boundary conditions are considered: (A) make $u_1=v_1=0$ and $\theta_1=0.1$ at node 1; (B) make $u_1=v_1=0$ at node 1 and $v_2=0.1$ at node 2. Within the scope of small deformation problems, both two cases will produce a rigid body rotation with constant rotational angle 0.1. As indicated in (Huang *et al.*, 2010), the original Allman's triangular element or other models in the same category cannot pass this test. It can be observed in Table 3 that the exact solutions can be obtained at all nodes by using this new element US-T3θ.

3.3 The torque test

In this test, the square plate shown in previous one is analyzed once again. As illustrated in Figure 5, two different cases are considered. In the first one, the center of this plate is completely fixed with $u_1=v_1=\theta_1=0$, and a pair of opposite forces are respectively imposed at the left and right vertexes. Then, the reaction moment acting on the DOF θ_1 is measured. In the second case, the plate is supported with $u_1=v_1=v_4=0$ and a twisting moment is imposed at the central node 1. Then the reaction force acting on the DOF v_4 is monitored. The numerical results listed in Table 4 verify that this new element can deliver exact solutions, proving its abilities for correctly undertaking the external in-plane twisting moments.

3.4 The short cantilever beam

Figure 6 depicts a short cantilever beam subjected to a parabolic shear force at the free end, with modulus $E=30000$, Poisson's ratio $\mu=0.25$ and thickness $t=1$. This beam will be firstly divided into $N\times2$ rectangles and each rectangle will be further modeled by two triangular elements, in which N indicates the subdivision number along the x-direction. In Figure 7, the convergence plots of the tip vertical deflections, which have been normalized by the reference solution 0.35601 (Felippa, 2003), are presented. It can be seen that the new element US-T3θ performs comparably well in this test.

3.5 The Cook's skew panel

In this test, the new triangular element is applied to the classical benchmark of Cook's skew panel

(Cook *et al.*, 1974), in that the structure behavior is dominated by shear deformation. This panel will also be modeled by $N \times N$ rectangles in which each rectangle is divided into two triangular elements. To study the element's sensitivities to mesh distortions, two different meshes will be considered here, i.e., the regular mesh and the irregular mesh, respectively as shown in Figure 8 (a) and (b). In Figure 9, the convergence curves of the tip vertical direction at point C, whose reference value is set as 23.965 (Cen *et al.*, 2015), are plotted. One can see that the results of the new element converge very rapidly.

3.6 The thin curved beam

As shown in Figure 10, the thin curved cantilever beam is subjected to a transverse shear force at its free tip. This beam will be successively modeled by using 6×1, 12×2 and 24×4 rectangle units, in which each rectangle contains two triangular elements. The convergence plots of the normalized tip vertical directions are given in Figure 11, in which the reference value is 0.08734 (Choo *et al.*, 2006). It is obvious that this new element exhibits much better performances than other triangular models in this test.

4. Conclusions

In this paper, a new simple but robust 3-node triangular membrane element with rational drilling DOFs is developed by the use of unsymmetric FEM. This unsymmetric element respectively adopts a conforming displacement field expressed in an elegant form to be the test functions, and a self-equilibrated stress field formulated based on the Airy stress solutions to be the trial functions. Besides, to make the element's drilling DOFs able to correctly present the true rotation in elasticity, certain constraint relations between theses drilling DOFs and the true rotations are introduced, generating a penalty stiffness which should be added to the normal stiffness. Moreover, special quadrature strategy is employed for future improvement of element performance. Numerical benchmarks reveal that this new element US-T3θ exhibits better capacities comparing with other triangular models. In particular, this element can correctly undertake the external in-plane twisting moments, thus is reasonable for formulating flat shell elements or being connected with other kind of elements with physical rotational DOFs.

Reference

Allman, D.J. (1984), "A compatible triangular element including vertex rotations for plane elasticity analysis", *Computers & Structures*, Vol.19, No. 1-2, pp.1-8.

Bathe, K.J. and Zhang, L. (2017), "The finite element method with overlapping elements-a new paradigm for CAD driven simulations", *Computers & Structures*, Vol.182, pp.526-539.

Boutagouga, D. (2017), "A new enhanced assumed strain quadrilateral membrane element with drilling degree of freedom and modified shape functions", *International Journal for Numerical Methods in Engineering*, Vol.110, No.6, pp.573-600.

Boutagouga, D. and Djeghaba, K. (2016), "Nonlinear dynamic co-rotational formulation for membrane elements with in-plane drilling rotational degree of freedom", *Engineering Computations*, Vol.33, No.3, pp.667-697.

Bucher, C. (2018), "A family of triangular and tetrahedral elements with rotational degrees of freedom", *Acta Mechanica*, Vol.229, No.2, pp.901-910.

Cen, S., Fu, X.R. and Zhou, M.J. (2011a), "8-and 12-node plane hybrid stress-function elements immune to severely distorted mesh containing elements with concave shapes", *Computer Methods in Applied Mechanics and Engineering*, Vol.200, No.29-32, pp.2321-2336.

Cen, S., Zhou, G.H. and Fu, X.R. (2012), "A shape-free 8-node plane element unsymmetric analytical trial function method", *International Journal for Numerical Methods in Engineering*, Vol.91, No.2, pp.158-185.

Cen, S., Zhou, M.J. and Fu, X.R. (2011b), "A 4-node hybrid stress-function (HS-F) plane element with drilling degrees of freedom less sensitive to severe mesh distortions", *Computers & Structures*, Vol.89, No.5-6, pp.517-528.

Cen, S., Zhou, P.L., Li, C.F. and Wu, C.J. (2015), "An unsymmetric 4-node, 8-DOF plane membrane element perfectly breaking through MacNeal's theorem", *International Journal for Numerical Methods in Engineering*, Vol.103, No.7, pp.469-500.

Choo, Y.S., Choi, N. and Lee, B.C. (2006), "Quadrilateral and triangular plane elements with rotational degrees of freedom based on the hybrid Trefftz method", *Finite Elements in Analysis and Design*, Vol.42, No.11, pp.1002-1008.

Cook, R.D., Malkus, D.S., Plesha, M.E. and Witt, R.J. (1974), *Concepts and Applications of Finite Element Analysis*, John Wiley & Sons.

Eom, J., Ko, J. and Lee, B.C. (2009), "A macro plane triangle element from the individual element test", *Finite Elements in Analysis and Design*, Vol.45, No.6-7, pp.422-430.

Felippa, C.A. (2003), "A study of optimal membrane triangles with drilling freedoms", *Computer Methods in Applied Mechanics and Engineering*, Vol.192, No.16-18, pp.2125-2168.

Fu, X.R., Cen, S., Li, C.F. and Chen, X.M. (2010), "Analytical trial function method for development of new 8-node plane element based on the variational principle containing Airy stress function", *Engineering Computations*, Vol.27, No.4, pp.442-463.

Huang, M., Zhao, Z. and Shen, C. (2010), "An effective planar triangular element with drilling rotation", *Finite Elements in Analysis and Design*, Vol.46, No.11, pp.1031-1036.

Leonetti, L., Garcea, G. and Nguyen-Xuan, H. (2017), "A mixed node-based smoothed finite element method (MNS-FEM) for elasticity", *Engineering with Computers*, Vol.33, No.4, pp.819-834.

Li, Z., Cen, S., Wu, C.J., Shang, Y. and Li, C.F. (2018), "High-performance geometric nonlinear analysis with the unsymmetric 4-node, 8-DOF plane element US-ATFQ4", *International Journal for*

Numerical Methods in Engineering, published online, https://doi.org/10.1002/nme.5771.

Liu, G.R., Dai, K.Y. and Nguyen, T.T. (2007), "A smoothed finite element method for mechanics problems", *Computational Mechanics*, Vol.39, No.6, pp.859-877.

Long, Y.Q. and Xu, Y. (1994), "Generalized conforming triangular membrane element with vertex rigid rotational freedoms", *Finite Elements in Analysis and Design*, Vol.17, No.4, pp.259-271.

Prathap, G., Manju, S. and Senthilkumar, V. (2007), "The unsymmetric finite element formulation and variational incorrectness", *Structural Engineering and Mechanics*, Vol.26, No.1, pp.31-42.

Rajendran, S. and Liew, K. (2003), "A novel unsymmetric 8-node plane element immune to mesh distortion under a quadratic displacement field", *International Journal for Numerical Methods in Engineering*, Vol.58, No.11, pp.1713-1748.

Rezaiee-Pajand, M. and Yaghoobi, M. (2014), "A robust triangular membrane element", *Latin American Journal of Solids and Structures*, Vol.11, No.14, pp.2648-2671.

Shang, Y. and Ouyang, W. (2018), "4-node unsymmetric quadrilateral membrane element with drilling DOFs insensitive to severe mesh-distortion", *International Journal for Numerical Methods in Engineering*, Vol.13, No.10, pp.1589-1606.

Shin, C.M. and Lee, B.C. (2014), "Development of a strain-smoothed three-node triangular flat shell element with drilling degrees of freedom", *Finite Elements in Analysis and Design*, Vol.86, No.2, pp.71-80.

Tang, L.M., Chen, W.J. and Liu, Y.X. (1980), "The quasi-conforming elements for finite element analysis", *Journal of Dalian University of Technology*, Vol.19, No.2, pp.19-35. (in Chinese)

Vu-Quoc, L. and Tan, X. (2013), "Efficient hybrid-EAS solid element for accurate stress prediction in thick laminated beams, plates, and shells", *Computer Methods in Applied Mechanics and Engineering*, Vol.253, pp.337-355.

Wang, C.S., Wang, Y., Yang, C.X., Zhang, X.K. and Hu, P. (2017), "8-node and 12-node plane elements based on assumed stress quasi-conforming method immune to distorted mesh", *Engineering Computations*, Vol.34, No.8, pp.2731-2751.

Wang, C.S., Zhang, X.K. and Hu, P. (2016), "New formulation of quasi-conforming method: A simple membrane element for analysis of planar problems", *European Journal of Mechanics-A/Solids*, Vol.60, pp.122-133.

Wisniewski, K. and Turska, E. (2012), "Four-node mixed Hu-Washizu shell element with drilling rotation", *International Journal for Numerical Methods in Engineering*, Vol.90, No.4, pp.506-536.

Zhou, P.L., Cen, S., Huang, J.B., Li, C.F. and Zhang, Q. (2017), "An unsymmetric 8-node hexahedral element with high distortion tolerance", *International Journal for Numerical Methods in Engineering*, Vol.109, No.8, pp.1130-1158.

Zouari, W., Hammadi, F. and Ayad, R. (2016), "Quadrilateral membrane finite elements with rotational DOFs for the analysis of geometrically linear and nonlinear plane problems", *Computers & Structures*, Vol.173, pp.139-149.

Table 1. Some 3-node and 6-node triangular element models for comparison

Symbol	Description	Reference
GT9	the generalized conforming element	(Long and Xu, 1994)
Allman	the classical Allman's triangular element	(Allman, 1984)
OPT	optimally fabricated assumed natural strain element	(Felippa, 2003)
SST	element based on strain states formulation	(Rezaiee-Pajand and Yaghoobi, 2014)
SM3	element with tuned higher-order stiffness parameter	(Eom *et al.*, 2009)
LST-Ret	retrofitted LST	(Felippa, 2003)
Huang	triangular element with reasonable drilling DOFs	(Huang *et al.*, 2010)
MNS-FEM	mixed node-based smoothed element	(Leonetti *et al.*, 2017)
HTD	hybrid Trefftz plane elements	(Choo *et al.*, 2006)
T6	the standard 6-node triangular isoparametric element	

Node	x	y	u ($\times 10^{-4}$)	v ($\times 10^{-4}$)	θ	σ_x	σ_y	τ_{xy}
1	0.00	0.00	0.00	0.00	0.00	**1333.333**	**1333.333**	**400.0**
2	0.24	0.00	2.40	1.20	0.00	**1333.333**	**1333.333**	**400.0**
3	0.24	0.12	3.00	2.40	0.00	**1333.333**	**1333.333**	**400.0**
4	0.00	0.12	0.60	1.20	0.00	**1333.333**	**1333.333**	**400.0**
5	**0.16**	**0.08**	**2.00**	**1.60**	**0.00**	1333.333	1333.333	400.0

Table 3. Results of the test for rigid body rotation

Node	1	2	3	4	5
Case A					
u	0.0	0.0	-0.1	0.0	0.1
v	0.0	0.1	0.0	-0.1	0.0
θ	**0.1**	**0.1**	**0.1**	**0.1**	**0.1**
Case B					
u	0.0	0.0	-0.1	0.0	0.1
v	0.0	0.1	0.0	-0.1	0.0
θ	**0.1**	**0.1**	**0.1**	**0.1**	**0.1**

Table 4. Results of the torque test

Case A	Numerical result	Reference solution
the reaction moment acting on the DOF θ_1	10.00	10.0
Case B		
the reaction force acting on the DOF v_4	5.00	5.0
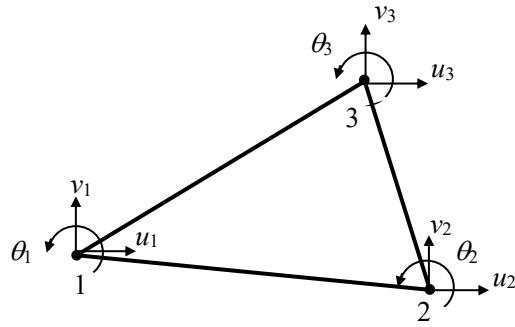
Figure 1. Unsymmetric 3-node 9-DOF triangular membrane element
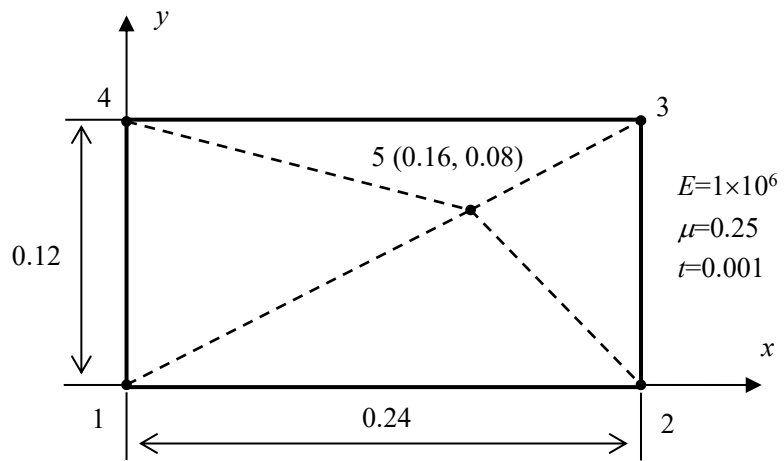
Figure 2. The patch test
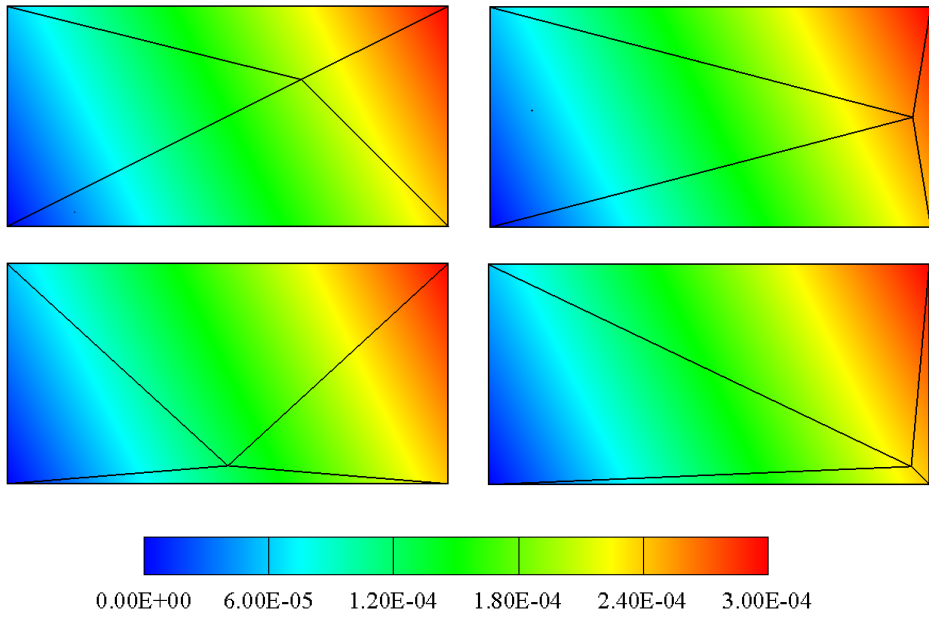
Figure 3. The contour plots of displacement u for the patch test
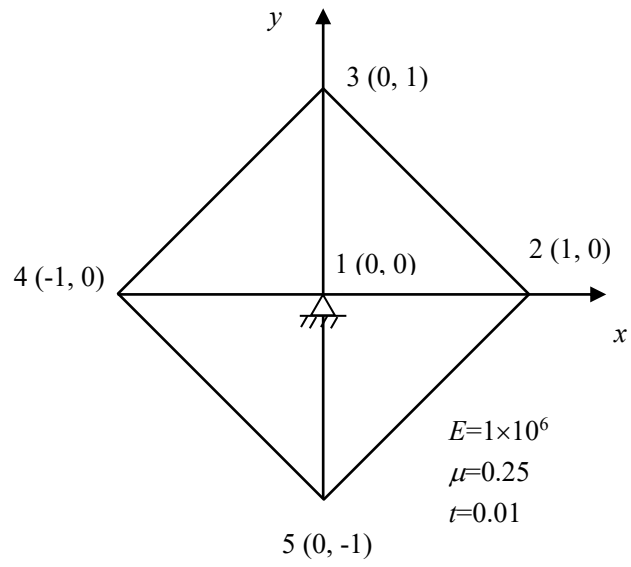
Figure 4. The test for rigid body rotation

(a) Case A (b) Case B
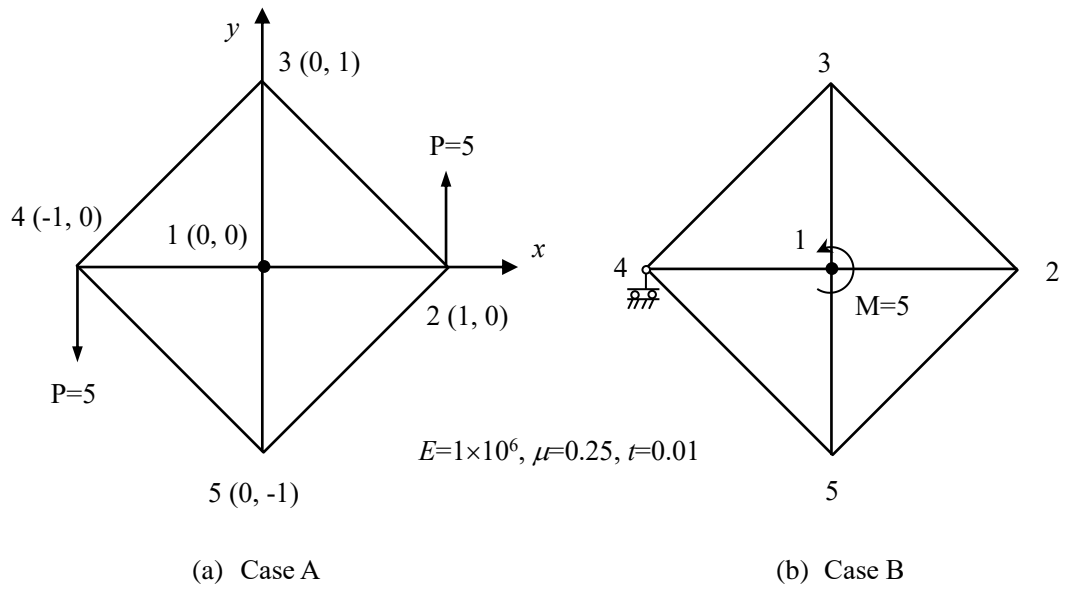
Figure 5. The torque test
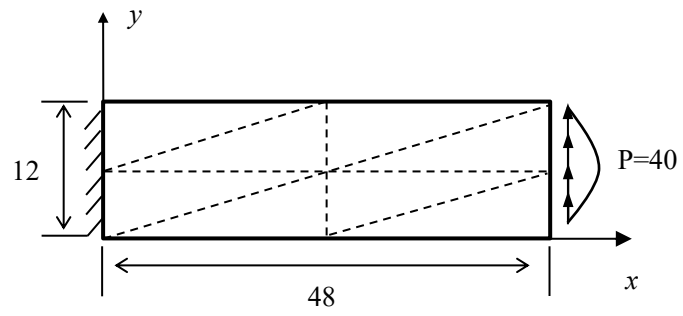
Figure 6. The short cantilever beam and the typical mesh 2×2
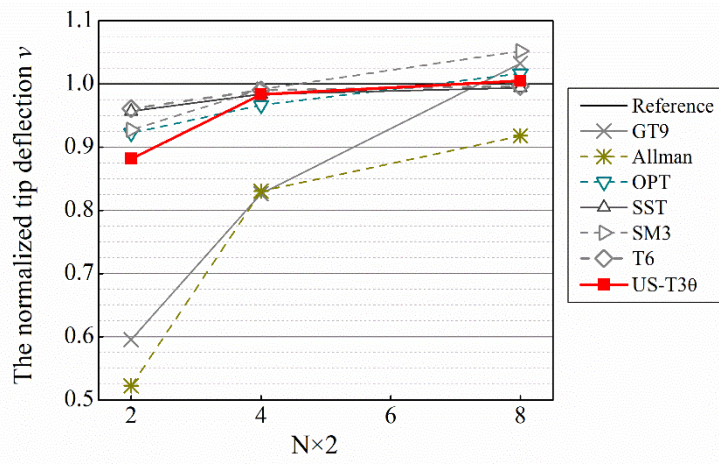
Figure 7. The tip deflection of the short beam
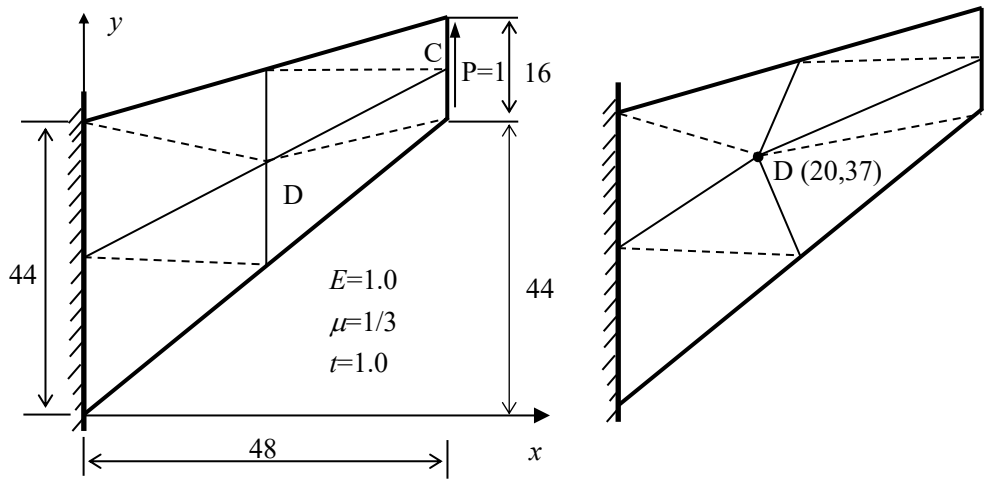
(a) Regular mesh (b) Irregular mesh
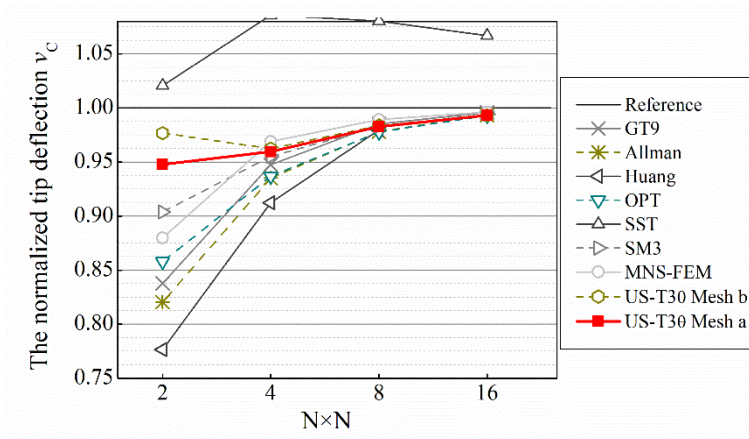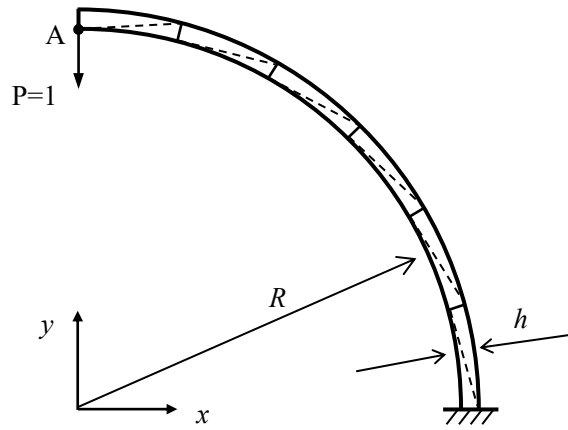
Figure 8. Cook's skew panel

Figure 9. The tip deflection v_c of Cook's skew panel

$R=4.12,\quad h=0.2,\quad E=10^7,\quad \mu=0.25,\quad t=0.1$
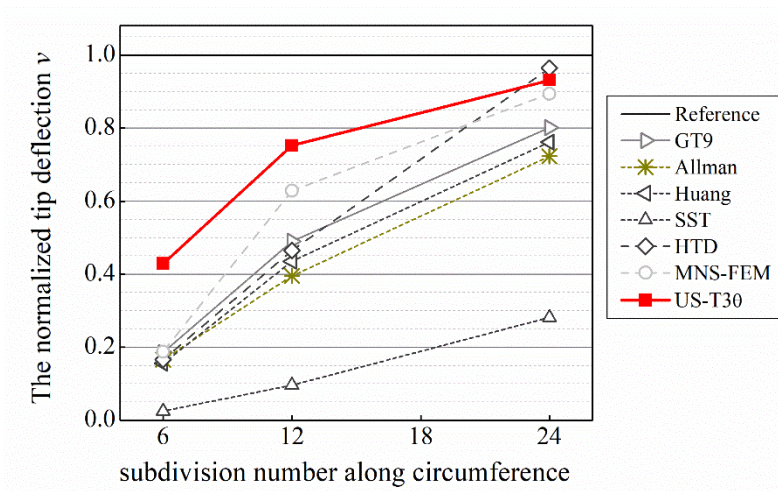
Figure 10. The thin curved beam and the typical mesh 6×1

Figure 11. The tip deflection of thin curved beam